

~~CONFIDENTIAL~~Copy 6
RM L52D07

NACA RM-L52D07

NACA

RESEARCH MEMORANDUM

SOME EFFECTS OF BODY CROSS-SECTIONAL SHAPE, INCLUDING A
SUNKEN-CANOPY DESIGN, ON DRAG AS SHOWN BY
ROCKET-POWERED-MODEL TESTS AT MACH
NUMBERS FROM 0.8 TO 1.5

By William E. Stoney, Jr., and Leonard W. Putland

Langley Aeronautical Laboratory
Langley Field, Va.

CLASSIFICATION CANCELLED

Authority: NACA Res. Abs. Date: 12/14/57

RN 26 94

By: MDA 1/18/56 Sec: _____

CLASSIFIED DOCUMENT

This material contains information affecting the National Defense of the United States within the meaning of the espionage laws, Title 18, U.S.C., Secs. 793 and 794, the transmission or revelation of which in any manner to an unauthorized person is prohibited by law.

NATIONAL ADVISORY COMMITTEE
FOR AERONAUTICS

WASHINGTON

July 1, 1952

~~CONFIDENTIAL~~

NATIONAL ADVISORY COMMITTEE FOR AERONAUTICS

RESEARCH MEMORANDUM

3 1176 01353 0440

SOME EFFECTS OF BODY CROSS-SECTIONAL SHAPE, INCLUDING A
SUNKEN-CANOPY DESIGN, ON DRAG AS SHOWN BY
ROCKET-POWERED-MODEL TESTS AT MACH
NUMBERS FROM 0.8 TO 1.5

By William E. Stoney, Jr., and Leonard W. Putland

SUMMARY

Free-flight tests were made with four fin-stabilized bodies of fineness ratio 8.91 to determine the effect of body cross-sectional shape on body drag at Mach numbers from 0.8 to 1.5 and Reynolds numbers from 15×10^6 to 50×10^6 . The configurations tested included two parabolic bodies of the same cross-sectional area, one circular and one elliptical. The third body had a nose section distorted to simulate a sunken-canopy configuration. The fourth model had the same cross-sectional area as the distorted-nose model but was circular in shape.

At supersonic speeds the small differences in drag between the models with the same longitudinal cross-sectional-area distributions substantiates the predictions of linearized theory that the first-order drag is independent of cross-sectional shape. As was also predicted by theory, the change in area distribution between the two pairs of models tested did not have any appreciable effect on the drag. In comparison with various bubble configurations previously tested, the sunken canopy added the same or less drag at supersonic speeds.

INTRODUCTION

The Pilotless Aircraft Research Division of the National Advisory Committee for Aeronautics is currently conducting an investigation to determine the drag of practical fuselage shapes at transonic and supersonic speeds. One phase of this program is concerned with drag differences due to changes in body cross-sectional shape while maintaining the same longitudinal distribution of cross-sectional area. This paper

presents comparisons of the drag for two pairs of models. The first pair consisted of two parabolic bodies, one having a circular cross section and the other having an elliptical cross section. The other pair consisted of one body with a simulated sunken canopy and one with a circular cross section having the same longitudinal area distribution as the sunken-canopy model.

The tests were conducted at the Pilotless Aircraft Research Station at Wallops Island, Va., with the use of rocket-propelled models. Data were obtained at Mach numbers from 0.8 to 1.5 and Reynolds numbers, based on body length, from 15×10^6 to 50×10^6 . The results are presented as curves of total drag coefficient against Mach number.

SYMBOLS

r	body radius at station x , inches
x	variable distance along body axis, measured from nose
R_m	maximum radius of body, 3.75 inches
L	length of body, 66.81 inches
M	Mach number
C_D	total drag coefficient, based on body frontal area
ΔC_D	incremental drag coefficient due to canopies, based on basic body frontal area
R	Reynolds number, based on body length
T_C	maximum frontal area of canopy in plane perpendicular to basic body profile
F_C	additional frontal area due to canopy
F_b	basic body frontal area

MODELS AND TESTS

The model configurations used in this investigation are shown in figure 1 and photographs of the models are shown in figure 2. All models were made of wood and finished to form a smooth and fair surface.

All models were stabilized by three 45° swept fins with a total exposed area of 1.69 square feet. The duralumin fins had a maximum thickness ratio of 0.0278 in the stream direction and were located on each body so that their trailing edges intersected the body at the 90.54-percent station.

Configuration 1 had a fineness ratio of 8.91 and the maximum diameter at the 40-percent station. The body had a circular cross section and its contour consisted of two parabolic arcs whose equations are as follows:

$$\frac{r}{R_m} = 1 - 6.25 \left(0.4 - \frac{x}{L} \right)^2 \quad 0 \leq \frac{x}{L} \leq 0.4 \quad (1)$$

$$\frac{r}{R_m} = 1 - 1.5631 \left(\frac{x}{L} - 0.4 \right)^2 \quad 0.4 \leq \frac{x}{L} \leq 1 \quad (2)$$

Configuration 2 had an elliptical cross section of ratio 1.5 to 1 and had the same cross-sectional-area distribution as that of configuration 1. The nose of configuration 3 was designed to represent a possible supersonic canopy configuration. Its coordinates are presented in figure 1(b). The afterbodies of configurations 3 and 4 were the same as that of configuration 1 as given in equation (2). The nose of configuration 4 had the same area distribution as that of configuration 3 but had a circular cross section. Its coordinates are also presented in figure 1(b).

Each model was propelled by a 5-inch HVAR light-weight booster rocket equipped with four fins and a 3.25-inch Mk. 7 sustainer rocket. The models were flown at the Pilotless Aircraft Research Station, Wallops Island, Va. All models were launched at an elevation angle of 70° .

Velocity data were obtained by tracking the models with the CW Doppler radar velocimeter and the NACA modified SCR 584 radar tracking unit as described in reference 1. Atmospheric data were obtained by radiosondes released at the time of firing. Drag coefficients have been based on body frontal area (0.307 square foot) and represent the total drag of the configurations including fin, base, and interference drag.

In figure 3, the Reynolds number during flight, based on body length, is plotted against Mach number for each body tested. The tests

covered a Reynolds number range of 15×10^6 to 50×10^6 . The Reynolds number range of model 1(a) was lower than that of the remaining models because it passed through the test Mach numbers at much higher altitudes than the other models since it was boosted by the more powerful 6-inch ABL Deacon booster rocket.

DISCUSSION OF ACCURACY

Two identical models of configurations 1 and 3 were flown and the drag coefficients obtained are presented in figures 4 and 5, respectively. The agreement shown between the drag of the models in each figure indicates the order of repeatability of the data. It should be noted here that figure 4 shows that the drag coefficients of configuration 1 were not affected by the large difference in Reynolds number between models 1(a) and 1(b). A survey of the drag data for 11 pairs of identical models flown previously showed that the largest C_D difference between identical models was 0.01. Thus, the difference shown between models 3(a) and 3(b) in figure 5 may be considered unusually large and, in general, a value of ± 0.01 may be taken as the probable error for the tests. This difference must be doubled when considering the accuracies of the canopy drags since they were obtained from the subtraction of the total drags of two models. The probable error in Mach number is mainly due to unknown wind velocities in the direction of the model flight path and is thus of a random nature. The results of numerous tests have shown it to be of the order of ± 0.01 . During the drag rise this difference can cause inaccuracies in C_D larger than those mentioned previously.

RESULTS AND DISCUSSION

In figure 6(a) the faired curve of drag coefficients for the parabolic body of circular cross section obtained from figure 4 is compared with the drag coefficients for the parabolic body of elliptical cross section. Figure 6(b) compares the drag coefficients of the distorted-nose model (faired from fig. 5) with those of the distorted-nose model with circular cross section. The differences for both pairs of models are within the order of accuracy of the tests over most of the supersonic range. In general, the differences shown between the drag coefficients of the models with the same longitudinal distribution of cross-sectional area substantiates the predictions of linearized theory (ref. 2) that, to the first order, the drag is dependent on the rate of change of area alone and is independent of the cross-sectional shape.

An estimate of the drag of both the circular distorted-nose configuration and the circular parabolic body at $M = 1.4$ is shown in figure 6. The drag coefficients for the various component parts were obtained as follows: The fin drag was measured in flight on a cylindrical body by use of the technique described in reference 1 and is presented in reference 3; the base drag was obtained experimentally in reference 4; the friction drag was estimated by the method of reference 5; the pressure drag was calculated by the method of Von Kármán and Moore (ref. 6) and, though the nose and afterbody pressure drags were different for the distorted and for the parabolic body, their total pressure drags were the same. Thus, the theory applied to one of each of the model pairs predicts that the total drag difference, caused by the different area distributions over the nose of the bodies, will be very small. The theory is substantiated by the results of the test since both pairs of curves lie within the band of accuracy of the tests.

In figure 7 the ratio of the elliptical to the circular parabolic body pressure drag at a Mach number of 1.4 is presented in comparison with similar ratios obtained by calculations made by the method of reference 7 of linearized characteristics for cones of elliptical and circular cross section. The experimental pressure drags were obtained by subtracting the fin, friction, and base drags (obtained as described previously) from the total drag coefficients shown in figure 6. Even though the difference in total drag between the elliptical and circular parabolic bodies lies within the accuracy band, it is interesting to note that the experimental ratio is of the same order as that shown by the theoretical calculations of cone pressure drags.

Previous tests (refs. 8 and 9) investigated the effect of bubble-type canopies on body drag. These results are presented in figure 8 together with the results for the simulated canopy model of the present paper. The incremental drag due to the various canopies is based on the basic body frontal area and is shown as a function of Mach number. The estimated values shown apply only to the models of reference 9

$\left(\frac{T_c}{F_b} = 0.106\right)$ and are the experimentally obtained drags of the bodies used as canopies.

As the plot shows, the sunken canopy added less drag than any of the bubble configurations at supersonic speeds. It must be mentioned, however, that the difference between the sunken canopy and the

$\frac{T_c}{F_b} = 0.106$ models was within the possible error of the tests. During transonic speeds the data are less reliable because of the fact that small errors in Mach number would cause large errors in ΔC_D values.

It is felt, however, that, whereas the levels of the curves in this range are somewhat in doubt, the trends shown are reliable and that the favorable interference shown for most of the canopies near Mach number 1 may be expected for bubble-type canopies located forward on the expanding-area part of sharp-nose bodies.

CONCLUSIONS

Flight tests at supersonic speeds and zero lift of two pairs of fin-stabilized bodies having the same longitudinal distribution of cross-sectional area lead to the following conclusions:

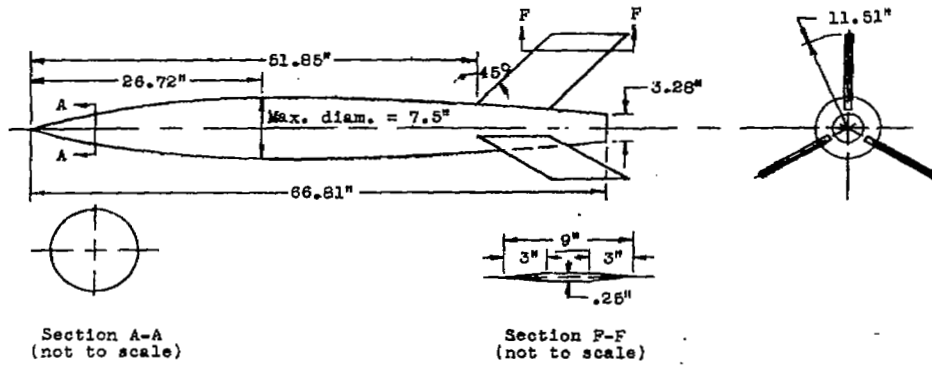
1. The small drag differences between the models with the same longitudinal cross-sectional-area distributions substantiates the predictions of linearized theory that, to the first order, drag is independent of cross-sectional shape. As was also predicted by theory, the change in area distribution between the two pairs of models tested did not have any appreciable effect on the drag.

2. In comparison with various bubble configurations previously tested, the sunken canopy added the same or less drag at supersonic speeds.

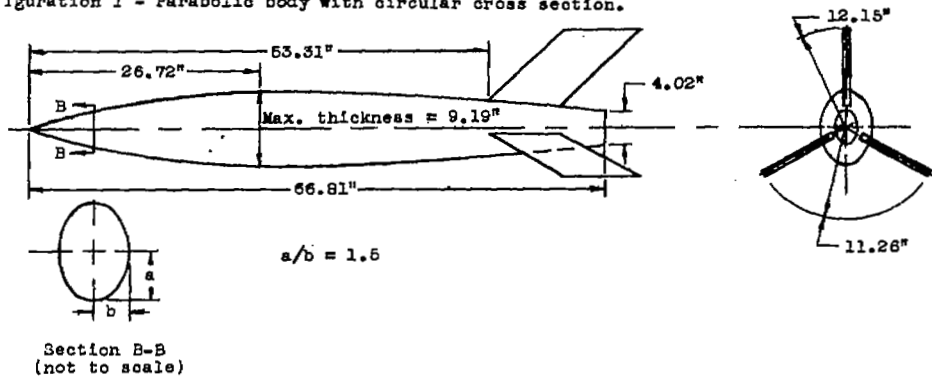
Langley Aeronautical Laboratory
National Advisory Committee for Aeronautics
Langley Field, Va.

REFERENCES

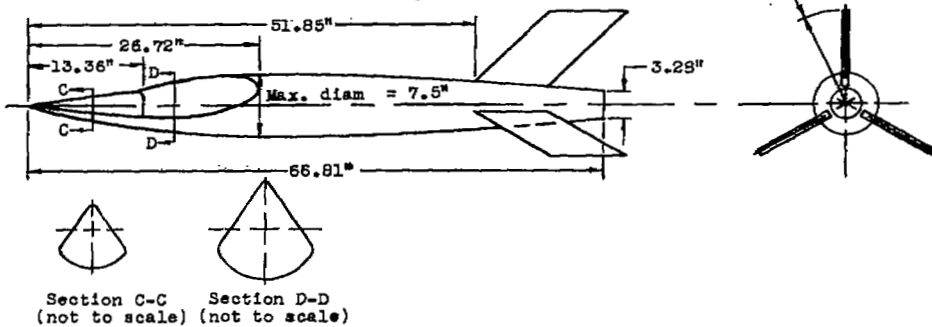
1. Morrow, John D., and Katz, Ellis: Flight Investigation at Mach Numbers From 0.6 to 1.7 To Determine Drag and Base Pressures on a Blunt-Trailing-Edge Airfoil and Drag of Diamond and Circular-Arc Airfoils at Zero Lift. NACA RM L50E19a, 1950.
2. Graham, Ernest W.: The Pressure on a Slender Body of Non-Uniform Cross-Sectional Shape in Axial Supersonic Flow. Rep. No. SM-13346-A, Douglas Aircraft Co., Inc., July 20, 1949.
3. Stoney, William E., Jr.: Pressure Distributions at Mach Numbers From 0.6 to 1.9 Measured in Free Flight on a Parabolic Body of Revolution With Sharply Convergent Afterbody. NACA RM L51L03, 1951.
4. Katz, Ellis R., and Stoney, William E., Jr.: Base Pressures Measured on Several Parabolic-Arc Bodies of Revolution in Free Flight at Mach Numbers From 0.8 to 1.4 and at Large Reynolds Numbers. NACA RM L51F29, 1951.
5. Van Driest, E. R.: Turbulent Boundary Layer in Compressible Fluids. Jour. Aero. Sci., vol. 18, no. 3, Mar. 1951, pp. 145-160, 216.
6. Von Kármán, Theodor, and Moore, Norton B.: Resistance of Slender Bodies Moving With Supersonic Velocities With Special Reference to Projectiles. Trans. A.S.M.E., vol. 54, no. 23, Dec. 15, 1932, pp. 303-310.
7. Ferri, Antonio: The Linearized Characteristics Method and Its Application to Practical Nonlinear Supersonic Problems. NACA TN 2515, 1951.
8. Alexander, Sidney R.: Effect of Windshield Shape of a Pilot's Canopy on the Drag of an NACA RM-2 Drag Research Model in Flight at Transonic Speeds. NACA RM L8E04, 1948.
9. Welsh, Clement J., and Morrow, John D.: Flight Investigation at Mach Numbers From 0.8 to 1.5 of the Drag of a Canopy Located at Two Positions on a Parabolic Body of Revolution. NACA RM L51A29, 1951.



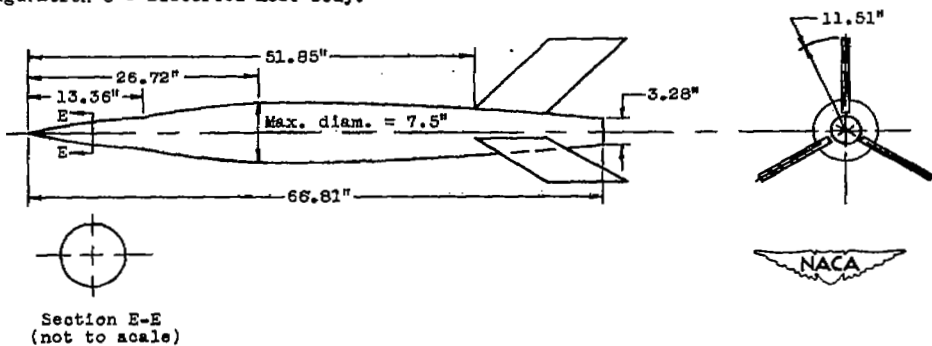
Configuration 1 - Parabolic body with circular cross section.



Configuration 2 - Parabolic body with elliptical cross section.



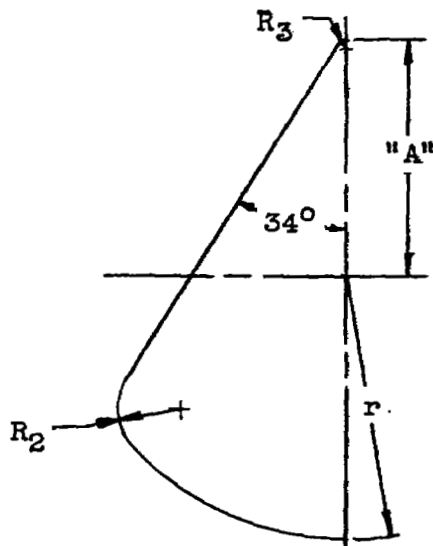
Configuration 3 - Distorted-nose body.



Configuration 4 - Distorted-nose body with circular cross section.

(a) Model configurations.

Figure 1.- General arrangement of test models.



Nose Dimensions				
Sta	r	R ₂	R ₃	"A"
0		0	0	0
1.07		0.29	0.29	0.29
2		.32		.40
4		.37		.65
6		.42		.89
8		.47		1.14
10		.51		1.38
12		.53	.29	1.63
13.36		.59	0	2.05
14		.61	0	2.28
16		.71	.11	2.84
18		.85	.53	3.21
20		1.05	1.11	3.43
22		1.35	1.79	3.61
24		1.82	2.60	3.71
26.72		3.75	3.75	3.75

Nose dimensions of distorted-nose body.

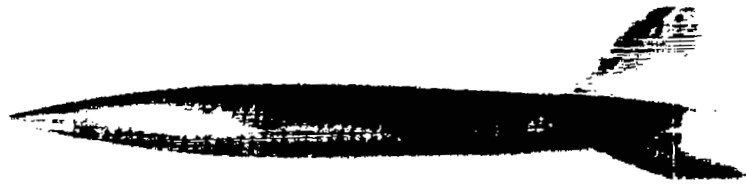
Nose Dimensions	
Sta	R
1.07	0.29
2	.44
4	.78
6	1.09
8	1.38
10	1.63
12	1.85
13.36	1.98
14	2.11
16	2.47
18	2.82
20	3.12
22	3.40
24	3.59
26.72	3.75

Nose dimensions of distorted-nose body
with circular cross section.



(b) Nose dimensions.

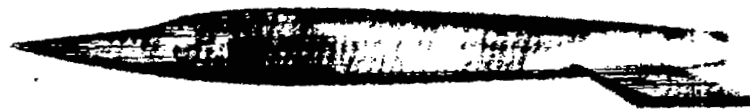
Figure 1.- Concluded.



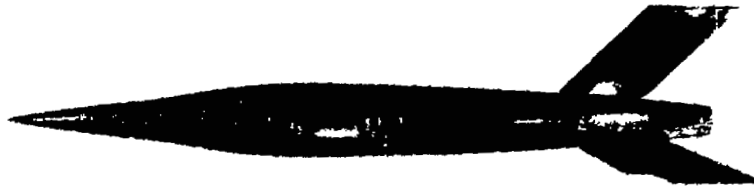
Circular-cross-section parabolic body.



Elliptical-cross-section parabolic body.



Distorted-nose body.

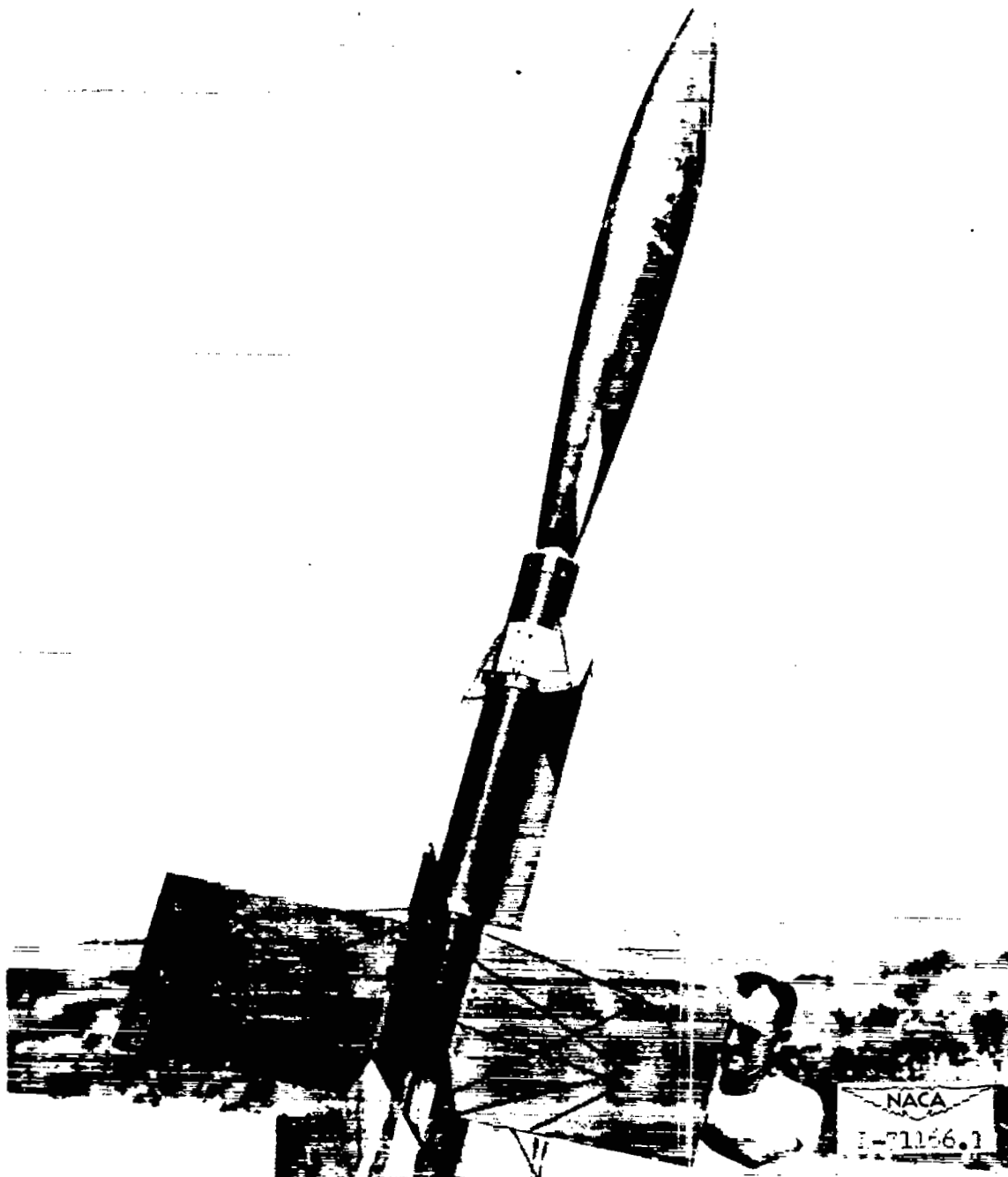


Circular-cross-section distorted-nose body.

(a) General views.

Figure 2.- Test models.


 NACA
L-74430



(b) Typical model-booster arrangement.

Figure 2.- Concluded.

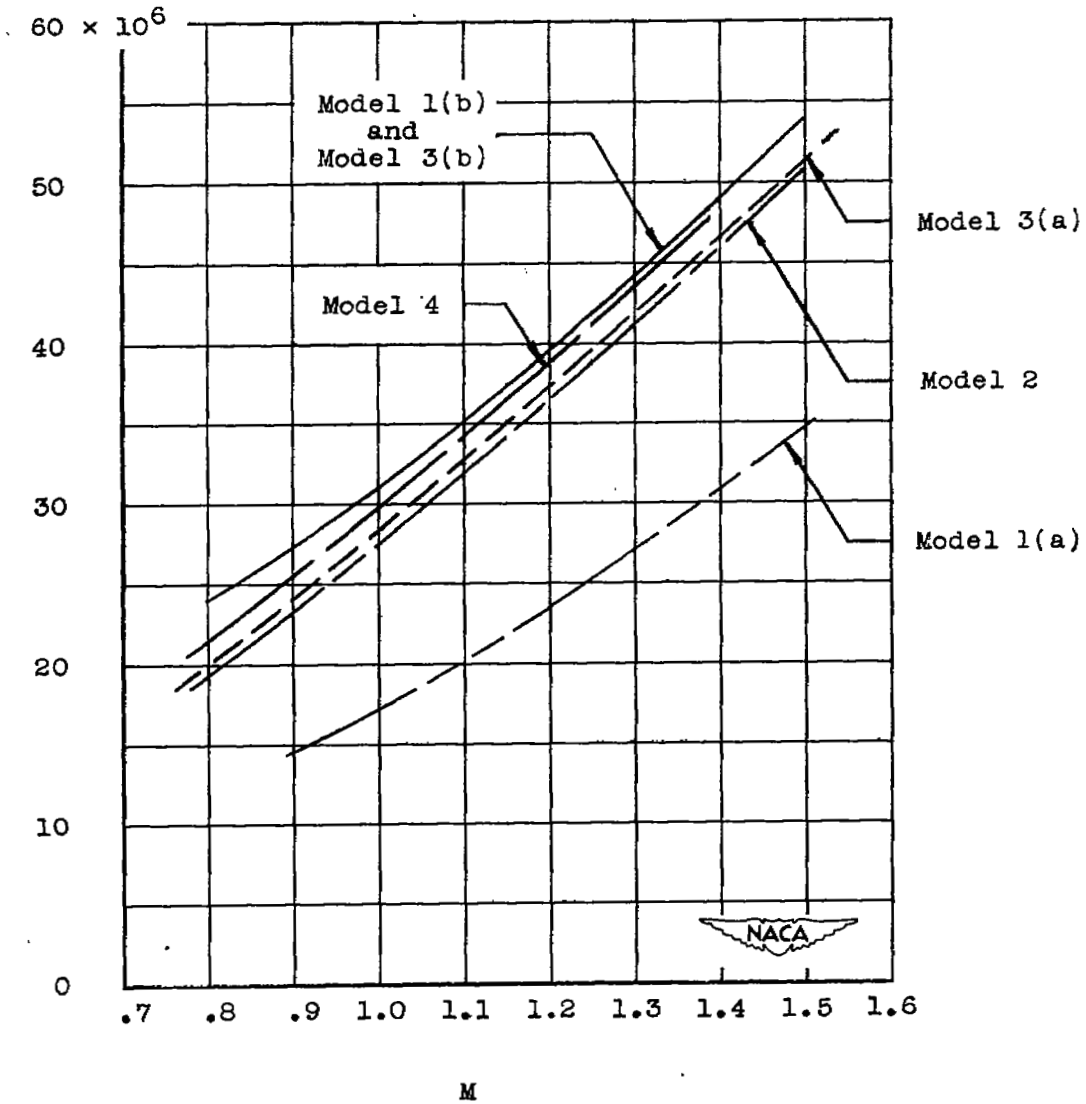


Figure 3.- Variation of Reynolds number in flight, based on body length, with Mach number for bodies tested.

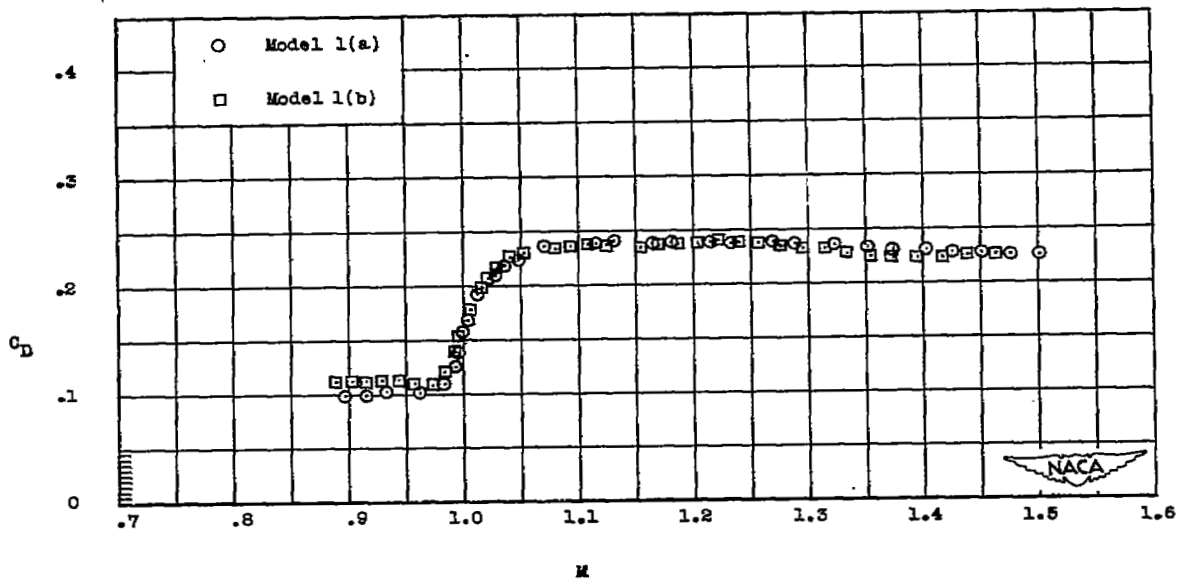


Figure 4.- Variation of drag with Mach number for identical models 1(a) and 1(b) with circular fuselage cross sections.

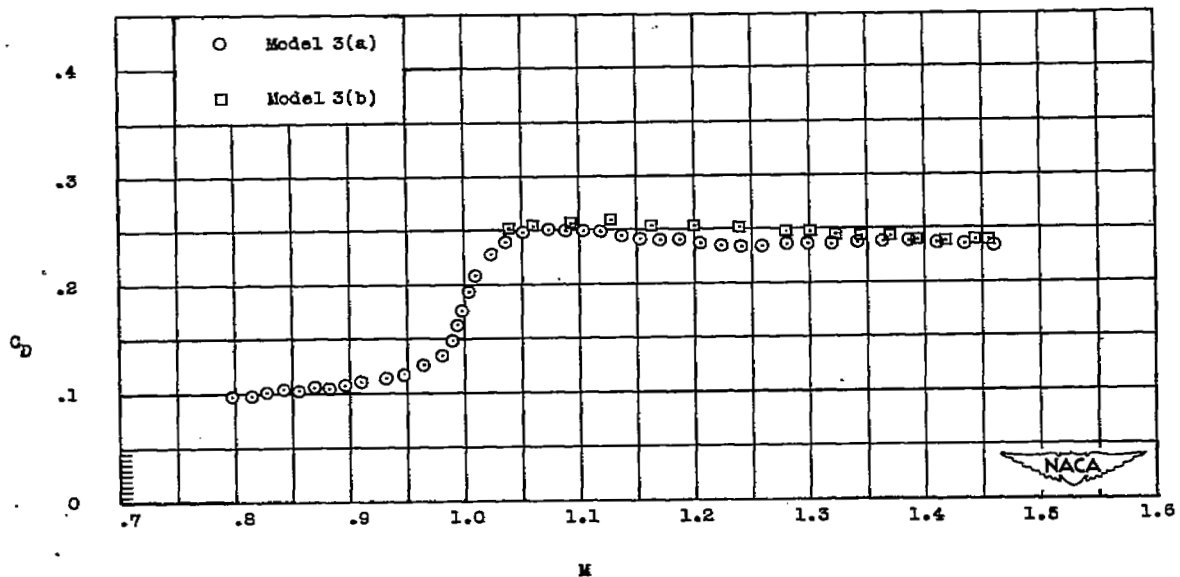
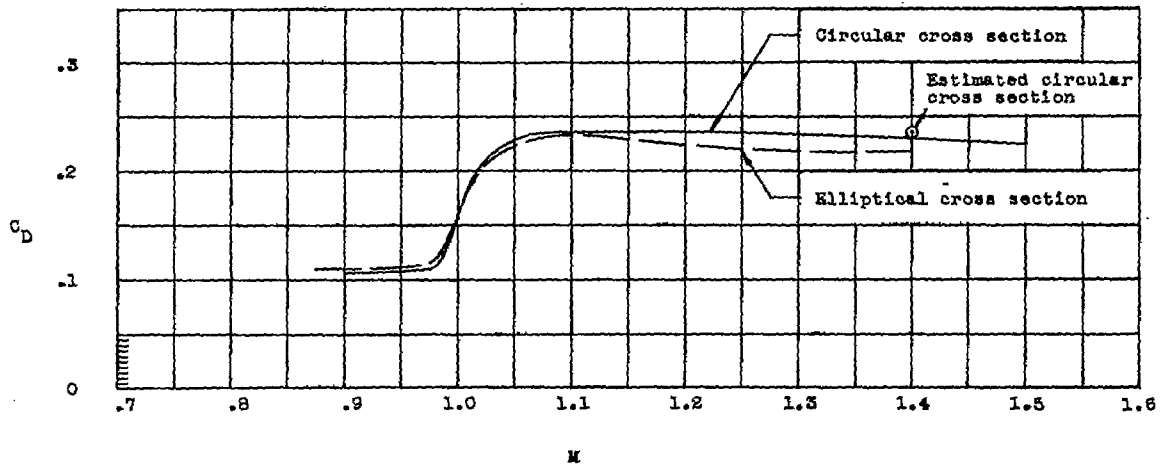
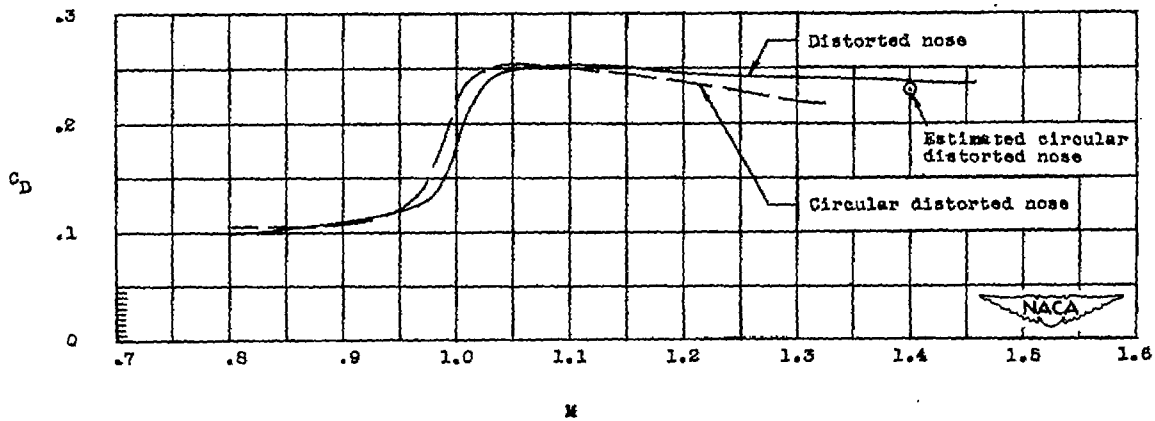


Figure 5.- Variation of drag with Mach number for identical models 3(a) and 3(b) with sunken canopies.



(a) Comparison of drag variation between a parabolic body with circular cross section and a parabolic body with elliptical cross section with the same cross-sectional area.



(b) Comparison of drag variation between a distorted-nose body and a distorted-nose body with circular cross section with the same cross-sectional area.

Figure 6.- Comparison of drag variation between models with the same cross-sectional area.

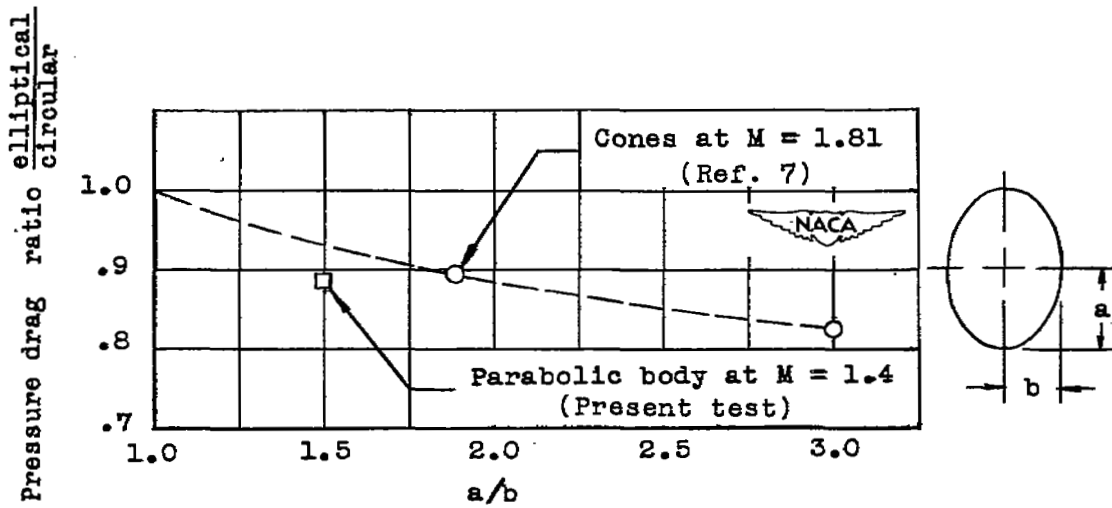


Figure 7.- Ratio of pressure drags for bodies of elliptical and circular cross sections.

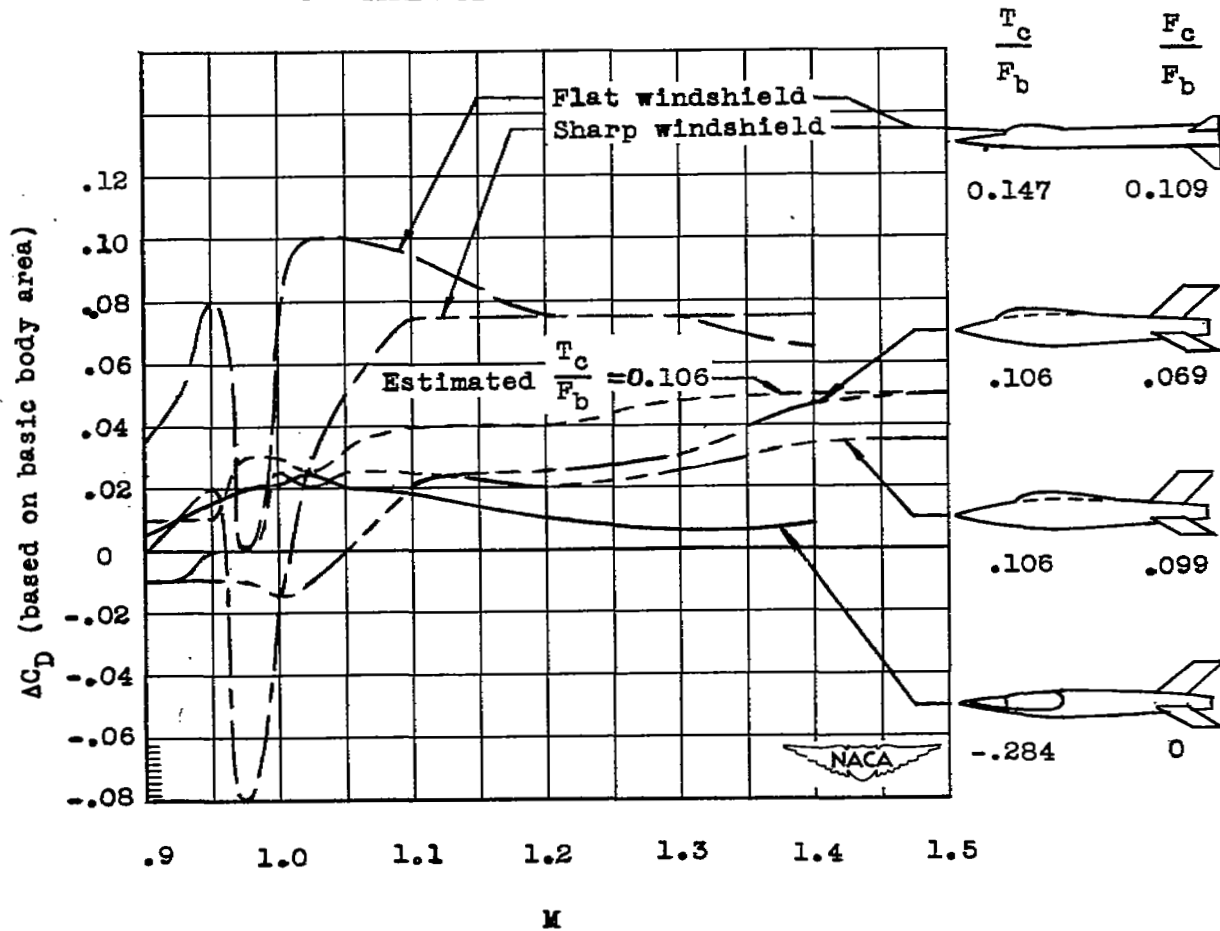


Figure 8.- Incremental drag of various canopy designs.

SECURITY INFORMATION

